

IDENTIFICATION OF A ROOT “SMART SPRING” SYSTEM FOR AUGMENTATION OF AEROELASTIC STABILITY OF A HELICOPTER ROTOR IN HOVER

M. Gennaretti[‡], L. Poloni[‡] and F. Nitzsche*

[‡]University Roma Tre
Dept. of Mechanical and Industrial Engineering
via della Vasca Navale 79
00146 Rome - Italy

*Carleton University
Dept. of Mechanical and Aerospace Engineering
1125 Colonel By Drive, ME 3242
Ottawa, Ontario, K1S 5B6 - Canada

Abstract

This work deals with an IBC based on inclusion of adaptive material at the root of hingeless helicopter rotor blades. Usually, IBC strategies involving the use of adaptive materials either consider adaptive material embedded in the blade structure for inducing strain deformations, or apply adaptive actuators for controlling segments of the blade (*e.g.*, for moving trailing-edge flaps). Here, the adaptive material is used to provide modal damping augmentation, and it may be tuned dependently of the actual rotor configuration to be stabilized. The presentation of a procedure for tailoring this ‘smart spring’ is the aim of the paper. The aeroelastic blade model considered consists of a cantilever slender beam undergoing flap, lead-lag and torsional motion, coupled with a strip-theory approach for the prediction of the aerodynamic loads, based on the very-low frequency approximation of the pulsating-free-stream Greenberg’s theory. Starting from this model and applying the Galérkin method, generalized mass, damping and stiffness matrices of the basic blade, as well as the incremental generalized mass, damping and stiffness matrices due to the ‘smart spring’ have been determined, the latter depending on the ‘smart spring’ inertial and elastic characteristics. It will be shown that, the application of an optimal control criterion, followed by a low-frequency-approximation observer, yields the identification of the most suitable ‘smart spring’ characteristics for augmentation of rotor blade aeroelastic stability. The validity of this procedure will be demonstrated by numerical results concerning the stability analysis of two different hovering blade configurations, with and without ‘smart spring’ inclusion.

1. Introduction

The helicopter industry is very much interested in the development of active control techniques to reduce noise and vibration of helicopters using smart structures. It is widely accepted that ‘smart’ structures have some of the most desired properties for aeroelastic control, but it is also recognized that they currently lack the capability to deliver sufficient power - defined as the maximum stroke multiplied by the delivered force divided by the actuation time - to provide the necessary control authority in most situations.

A worldwide research effort to develop ‘smart’ aeroservoelastic systems is underway. Unfortunately, materials such as shape memory alloys (SMA) that have the capability to overcome the work done by typical aerodynamic loads encountered in flight provide poor bandwidth. Conversely, materials that have good dynamic response lack sufficient displacement capability (such as the piezoelectric crystal PZT, the piezoelectric film PVDF, and the electrostrictive or magnetostrictive materials). Nevertheless, due to their dynamic response characteristics, PZT, electrostrictive and magnetostrictive materials are the best candidates to fulfill the active control requirements of aeroelastic systems. These materials have high stiffness and can deliver relatively large forces but only over a very limited stroke (approximately 300 m-strain for PZT and electrostrictive materials, and 1,000 m-strain for magnetostrictive materials). Although the stroke may be amplified by mechanical means, a corresponding reduction in the actuation force becomes an unavoidable trade-off. The most investigated approach to overcome the material limitations and to achieve aeroelastic control using

‘smart’ structures is based on the deflection of aerodynamic surfaces actuated by beams constructed with stacked PZT or bimorphs [1]. Another approach that is receiving attention from the research community uses piezoelectric fibers to directly alter the blade camber [2]. However, all these different solutions cannot demonstrate very significant changes in the local angle of attack and, in general, low control authority is achieved [3]. The ‘smart spring’ that is investigated in the present work is an alternate approach to achieving aeroelastic control, which exploits the large stiffness, force and bandwidth of the aforementioned materials, and circumvents their lack of power.

The primary advantage in the ‘smart spring’ system, compared to other active control systems that are available, is that the device does not rely on achieving high stroke and force simultaneously. Hence, the resultant mechanical work required for control is kept relatively small. Rather, the device only requires the actuators to produce micro displacements to generate friction forces between two structural members and engage a structural reinforcement in the load path. This scheme avoids the fundamental problems of other control schemes that require high displacement and force to act simultaneously, increasing the mechanical work necessary to achieve full control authority.

The ‘smart spring’ concept

The ‘smart spring’ uses the high stiffness and good time response characteristics of the PZT, electrostrictive or magnetostrictive materials to dynamically control the cross-section stiffness of typical aeronautical structures [4]. The stiffness of the original structure is altered in time by engaging the reinforcement in the load path as seen in the conceptual sketch shown in Figure 1. As the reinforcement is engaged, the stiffness of the structure increases to a maximum value in one half of the control cycle. In the subsequent half-cycle, the stiffness decreases to the original baseline value by removing the reinforcement from the load path. The waveform that characterizes the change in stiffness between these two levels during one complete cycle resembles a step function smothered by the dissipation effects that are produced by the contact friction between the surfaces of the reinforcement and the stopper located in the main structure.

The main parameters that appear in the design of a ‘smart spring’ are: (1) the baseline stiffness that determines the elastic deformation of the original

structure without the ‘smart spring,’ (2) the amplitude of stiffness variation required by the active control relative to the baseline value, and (3) the force required to generate friction, engage the reinforcement and guarantee continuity in the load path. Since the engagement is done by friction between the reinforcement and the stopper, the stiffness variation is in an actual ‘smart spring’ a complex-valued function. It presents a hysteretic loop during the load/unloading cycle of the actuator as the whole structure vibrates and relative motion between the stopper and the reinforcement is present.

It is worthwhile to point out that the mechanical work necessary to engage the reinforcement in the device is orthogonal to the work delivered by the external loads. Therefore, control over the external loads is achieved indirectly, inserting and removing the reinforcement from the load path. Although the active material needs to deliver a relatively large force in this configuration, the required stroke to guarantee the load path continuity is minimum, within the fabrication tolerances, and well below the limits of the typical ‘smart’ material displacement capabilities. The ‘smart spring’ is a useful concept particularly when dynamic loads are present since relatively large variations in the mechanical impedance of the system can be achieved over time [5].

One important application for the ‘smart spring’ is in helicopter rotor individual blade control (IBC). In any active control technique applied to helicopters, a judicious redistribution of the aerodynamic spectrum, as seen by the rotating blade, is the key issue to be addressed. IBC, according to its original and broad definition of a rotating frame actuation scheme, can be implemented in different ways [6]. Using the options available at the moment, one may command a pitch to the blade root by hydraulic actuators, use a ‘smart’ flap located near the blade tip, or still provide torsion deformations on the blade via embedded piezoelectric fibers. However, in order to generate significant changes in the aerodynamic spectrum and provide enough control authority, relatively large pitch deflections are necessary. This is one of the main technical reasons that prevented the use of ‘smart’ structures solutions in full-size helicopter rotors. Under this scope, another valid implementation of IBC is to actively adapt the stiffness of the blade structure by changing its sectional moment of area in time. In this case, the aeroelastic response characteristics of the blade will change in time like in the gust alleviation problem associated with fixed wings.

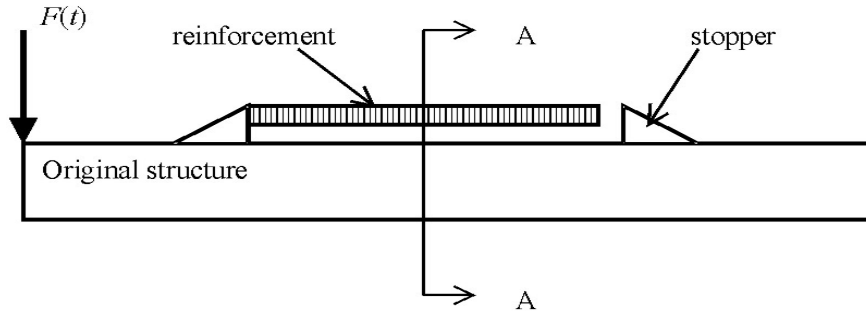


Figure 1: Concept of active stiffness control (the ‘smart spring’) applied to a simple beam cross section, denoted by A-A. The gap (exaggerated) between the stopper and the reinforcement made from a stack of piezoelectric wafers is closed when the electric field is applied. The moment reaction at the boundary of the original structure, due to the external force, is indirectly controlled by the cyclic control of the cross-sectional stiffness.

The ‘smart spring’ described in the present work can alter the mechanical impedance of the dynamic system introducing a form of active control similar to the one provided by tunable vibration absorbers (TVA) whose stiffness or gain characteristics can be scheduled. Therefore, tailoring the aeroelastic response of each blade to perform IBC using active control is feasible by the proper choice of a control law. In fact, the hardware of ‘smart spring’ can be used to control phenomena associated with different bands of the vibration spectrum, such as low frequency vibration trans-

missibility throughout the rotor hub, blade vortex interaction and dynamic stall effects. In the present work the ‘smart spring,’ as an example of control objective, is used to provide modal damping augmentation.

A prototype of the ‘smart spring’ is undergoing preliminary tests in still air at the National Research Council of Canada (NRCC) [7]. This proof-of-concept model was designed to actuate mainly in the torsional degree of freedom of the blade for simplicity.

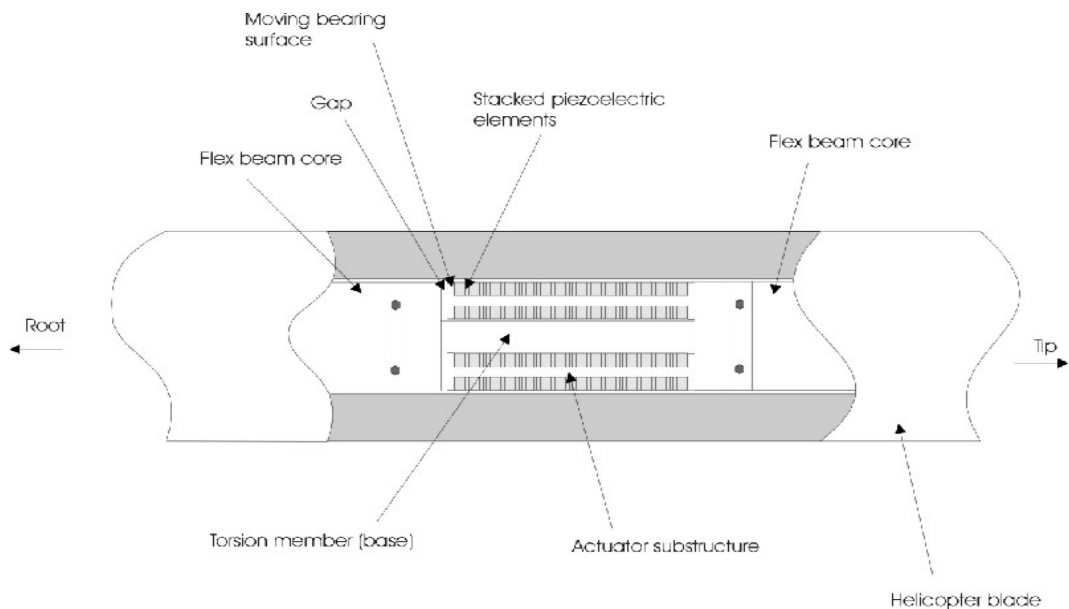


Figure 2: Schematic of ‘smart spring’ at the blade root.

The design of the ‘smart spring’ that is undergoing tests at NRCC uses stacked PZT actuators to activate three additional load paths or reinforcements near the blade root (Figure 2). The frictional forces generated by actuation of the stacked PZT enables the engagement of the additional load carrying members to alter the blade overall torsional stiffness. The operation of the actuators provides real-time alteration of the cross-sectional stiffness at the blade root. It is recognized that any small change in the boundary conditions affects very much the overall aeroelastic response of the blade. This prototype of ‘smart spring’ consists of an array of sensors, such as accelerometers, a signal analyzer, a computer, and piezoelectric stacked actuators assembled in the three cans - the reinforcements (Figure 3). The baseline blade stiffness is maintained through the ‘smart spring’ device using a central torsion member. This torsional member closely matches the original blade torsional stiffness and sustains primary load path throughout the system. Sensors such as accelerometers are embedded along the blade to provide the vibration information to the control computer, which analyzes these signals, performs system identification and generate the control signal to the piezoelectric actuators to achieve vibration attenuation.

Tailoring of the ‘smart spring’

In this work, the adaptive material placed at the blade root is applied for blade stability augmentation by tuning its stiffness dependently of the

actual rotor configuration. We present a formulation that, for a given hovering rotor configuration (*e.g.*, for fixed collective-pitch and pre-cone angles) yields the optimal tailoring of the ‘smart spring’ (*i.e.*, it gives the ‘smart spring’ parameters to be tuned at each configuration). It is inspired to the approach introduced in [8], where the authors investigated about stabilizing effects induced by the root ‘smart spring’, when used as a harmonic parametric excitation device. Specifically, following Ref. [9], the aeroelastic model is obtained considering an untwisted cantilever slender beam, undergoing flap bending, chordwise bending and torsion, with mass, tensile and aerodynamic axes coinciding with the elastic axis, coupled with the aerodynamic loads predicted by a strip-theory model based on the very-low frequency approximation of the pulsating-free-stream Greenberg’s extension of the Theodorsen theory [10]. Starting from this model and applying the Galérkin approach, generalized mass, damping and stiffness matrices of the basic blade, as well as the incremental generalized mass, damping and stiffness matrices due to the ‘smart spring’ have been determined, the latter depending on the ‘smart spring’ inertial and elastic characteristics (see Section 2). Then, the ‘smart spring’ elastic characteristics that are most suitable for the augmentation of rotor blade aeroelastic stability, have been evaluated by applying an optimal control criterion, followed by a low-frequency-approximation observer (see Section 3).

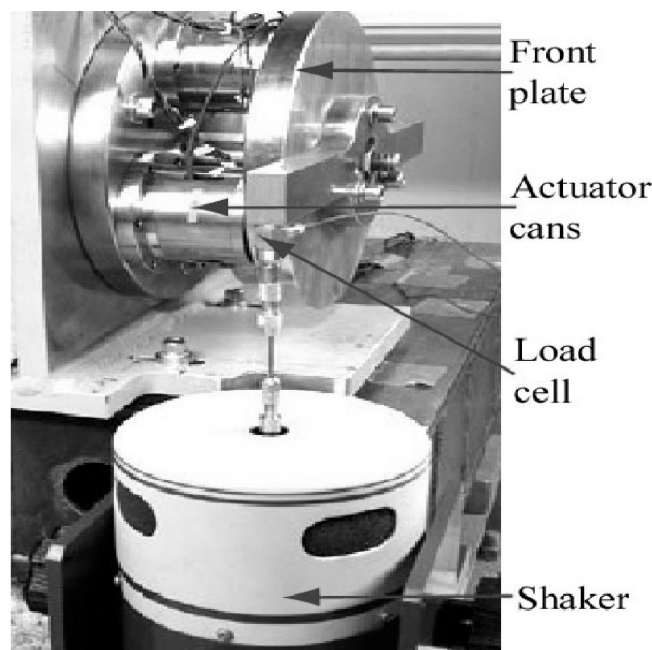


Figure 3: ‘Smart spring’ tunable vibration absorber (TVA) being tested at the NRC facilities in Ottawa, Canada.

As a validation of the methodology presented, we will present numerical results concerning the stability-augmentation effect of the ‘smart spring’ on two different hovering blade configurations.

2. Smart-blade aeroelastic model and solution procedure

Following the approach presented by Hodges and Ormiston [9], the basic-blade aeroelastic model (*i.e.*, that with no ‘smart spring’ inclusion) has been derived by applying the structural blade model introduced by Hodges and Dowell [11] to a uniform blade, and combining it with the unsteady aerodynamic model obtained from the very-low frequency approximation of the pulsating-free-stream Greenberg extension of the Theodorsen theory for airfoils in incompressible flow [10].

In this model, the blade is assumed to be a slender, straight beam with the elastic axis undergoing axial deformation, $u(x, t)$, lateral in-plane displacement (lead-lag bending), $v(x, t)$, and lateral out-of-plane displacement (flap bending), $w(x, t)$, whereas cross-sections are subject to torsion deformation, $\phi(x, t)$, about it. In Ref. [11], the structural equations are derived after application of an ordering scheme procedure based on the restriction that the squares of the bending slopes, torsion deformation, chord/radius and thickness/radius ratios were small with respect to unity. A further simplification of the model is obtained by solving for $u(x, t)$ in terms of local tension and assuming that radial displacements are simply geometric consequences of the transverse bending deflections. The final form of the structural model is a set of nonlinear, coupled, integro-partial differential equations that can be applied to rotor blades undergoing moderate displacements (see Refs. [11] and [9] for details).

Here, this model has been modified in order to include the effects of the ‘smart spring’ on the blade structural dynamics. In particular, geometric, mass and elastic characteristics of the blade have been expressed as discontinuous (generalized) functions of the blade spanwise direction, through a hat function accounting for the ‘smart spring’ presence. Indeed, if x denotes the abscissa along the blade span, and α is a generic blade parameter that is altered by the ‘smart spring’ located between x_1 and x_2 ($x_1 < x_2$), we have

$$\alpha(x) = \alpha_0(x) + \Delta H(x, x_1, x_2) \alpha_s$$

where, for H denoting the Heaviside function, $\Delta H(x_1, x_2) = H(x - x_1) - H(x - x_2)$ is the hat function, α_s is the incremental value due to the

‘smart spring’ and α_0 is the basic-blade parameter. Then, following this criterion, equations given in Ref. [11] have been manipulated so as to get three novel nonlinear, integro-partial differential equations of smart blade dynamics, that may be synthesized in the following form (see Appendix A and Ref. [12] for details):

$$\begin{aligned} m \ddot{v} + \mathcal{O}_v[v, w, \phi, E_0, E_s] &= \mathcal{L}_v \\ m \ddot{w} + \mathcal{O}_w[v, w, \phi, E_0, E_s] &= \mathcal{L}_w \\ J \ddot{\phi} + \mathcal{O}_\phi[v, w, \phi, E_0, E_s, G_0, G_s] &= \mathcal{M}_\phi, \end{aligned}$$

where m denotes the blade mass per unit length, J denotes the cross-section torsional mass moment of inertia, E denotes the Young modulus, G denotes the shear modulus, \mathcal{O}_v and \mathcal{O}_w denote fourth-order in space, nonlinear, integro-partial differential operators, whereas \mathcal{O}_ϕ denotes a second-order in space, nonlinear, partial differential operator. Note that, the nonlinear operators \mathcal{O}_v , \mathcal{O}_w , and \mathcal{O}_ϕ include both the inertial effects due to the blade rotational speed, and the influence of the ‘smart spring’ presence through the generalized hat function, ΔH . Furthermore, \mathcal{L}_v and \mathcal{L}_w are, respectively, the in-plane and out-of-plane aerodynamic forces per unit length acting on the blade, whereas \mathcal{M}_ϕ is the aerodynamic pitching moment per unit length. As already mentioned, these loads have been predicted by the quasi-steady Greenberg theory, with the effects of the wake-induced velocity (important in hovering rotor configurations) taken into account by modifying the direction of the aerodynamic forces. The final aeroelastic model is achieved by expressing in terms of $v(x, t)$, $w(x, t)$ and $\phi(x, t)$, the airfoil velocity components appearing in the quasi-steady expression of \mathcal{L}_v , \mathcal{L}_w and \mathcal{M}_ϕ given by the Greenberg theory.

Modal-approach solution

The rotor blade aeroelastic solution has been obtained by following the approach presented in Ref. [9]. It consists of a three step procedure: first, the Galérkin method is applied for the spatial integration of the coupled, integro-partial differential aeroelastic equations, then, the trim blade configuration is determined by solving the nonlinear algebraic problem resulting from steady-state assumption, and finally, the aeroelastic behavior is determined through analysis of the linearized equations of the dynamics of small perturbations about trim.

Specifically, in the first step, the elastic blade deflections are expressed as

$$v(x, t) = \sum_{n=1}^N q_n^v(t) \Psi_n^v(x),$$

$$w(x, t) = \sum_{n=1}^N q_n^w(t) \Psi_n^w(x),$$

$$\phi(x, t) = \sum_{n=1}^N q_n^\phi(t) \Psi_n^\phi(x),$$

where $\Psi_n^v, \Psi_n^w, \Psi_n^\phi$ are sets of linearly-independent shape functions (eigenfunctions of a cantilever nonrotating beam, in our case), whereas q_n^v, q_n^w, q_n^ϕ denote the generalized coordinates of the problem (modal amplitudes). Substituting these expressions in the aeroelastic integro-partial differential equations, and applying the Gal rkin method yields a set of $3N$ nonlinear, ordinary differential equations in terms of the generalized coordinates of the problem. Then, the dynamics of the generalized coordinates is expressed as combination of a steady-state condition with a small-perturbation term, *i.e.*, $q_n^v(t) = q_{0n}^v + \Delta q_n^v(t)$, $q_n^w(t) = q_{0n}^w + \Delta q_n^w(t)$, and $q_n^\phi(t) = q_{0n}^\phi + \Delta q_n^\phi(t)$. Substituting the steady-state values into the nonlinear differential equations, one obtains a set of $3N$ nonlinear algebraic equations, that can be solved in order to determine the trim modal amplitudes $q_{0n}^v, q_{0n}^w, q_{0n}^\phi$. Finally, subtracting the steady-state equations from the complete nonlinear differential equations, dropping all terms that are nonlinear in the perturbation quantities, one obtains a set of $3N$ linear ordinary differential equations governing perturbations about trim, of the following type

$$\begin{aligned} & [\mathbf{M}(\mathbf{q}_0) + \Delta\mathbf{M}(\mathbf{q}_0, m_s, J_s)] \ddot{\mathbf{q}} + \\ & [\mathbf{C}(\mathbf{q}_0) + \Delta\mathbf{C}(\mathbf{q}_0, m_s)] \dot{\mathbf{q}} + \\ & [\mathbf{K}(\mathbf{q}_0) + \Delta\mathbf{K}(\mathbf{q}_0, m_s, J_s, \lambda_s^y, \lambda_s^z, \kappa_s)] \mathbf{q} = \mathbf{0}, \end{aligned} \quad (1)$$

where \mathbf{q} denotes the vector of the $3N$ perturbation generalized coordinates. Note that, in equation (1) the global aeroelastic mass, damping and stiffness matrices have been decomposed in the portion that describe the basic-blade dynamics ($\mathbf{M}, \mathbf{C}, \mathbf{K}$), and in the additional matrices due to the presence of the ‘smart spring’ ($\Delta\mathbf{M}, \Delta\mathbf{C}, \Delta\mathbf{K}$). Due to the nonlinear nature of the problem, both basic-blade and ‘smart spring’ matrices depend on the trim solution, \mathbf{q}_0 . Furthermore, all ‘smart spring’ matrices depend on the ‘smart spring’ mass parameters, m_s and J_s , whereas the stiffness matrix, $\Delta\mathbf{K}$, depends also on the nondimensional additional lead-lag bending stiffness, λ_s^z , flap bending stiffness, λ_s^y , and torsional stiffness, κ_s , due to the ‘smart spring’ (see Ref. [12] for details).

3. Optimal ‘smart-spring’ stiffness

Observing that, once a given piezoelectric element is located on the blade its inertial effects on the

blade dynamics are fixed, the objective of this section is the presentation of an algorithm for the identification of the incremental blade stiffness parameters due to the presence of the ‘smart spring’, namely $\lambda_s^y, \lambda_s^z, \kappa_s$, that are capable to enhance the stability behavior of the ‘smart’ blade, with respect to that of the basic one.

To this aim, for fixed m_s and J_s , we recast equation (1) in the following form

$$\hat{\mathbf{M}} \ddot{\mathbf{q}} + \hat{\mathbf{C}} \dot{\mathbf{q}} + \mathbf{K} \mathbf{q} = -\Delta\mathbf{K}(\lambda_s^y, \lambda_s^z, \kappa_s) \mathbf{q}, \quad (2)$$

where matrices $\hat{\mathbf{M}}, \hat{\mathbf{C}}$ and \mathbf{K} depend on trim blade deformation and ‘smart spring’ mass parameters. In equation (2), it is apparent that the contribution of the ‘smart spring’ stiffness yields a sort of structural feedback, that we wish to use as an aeroelastic stabilizer. Hence, starting from this observation, in order to identify a convenient matrix $\Delta\mathbf{K}$, first, we replace the ‘smart spring’ stiffness terms with a set of fictitious generalized forces, \mathbf{f} , that assume the role of control variables. Then, using optimal control criteria, we determine the stabilizing feedback gain matrix that relates \mathbf{f} to the blade generalized coordinates, and finally identify $\lambda_s^y, \lambda_s^z, \kappa_s$ such that $\Delta\mathbf{K}$ yields a feedback that is as close as possible to that provided by the optimal gain matrix assuring stabilization.

Specifically, replacing ‘smart spring’ stiffness terms with the fictitious control variables, \mathbf{f} , and recasting in state-space form, equation (2) becomes

$$\dot{\mathbf{x}} = \mathbf{A} \mathbf{x} + \mathbf{B} \mathbf{f}, \quad (3)$$

where $\mathbf{x}^T = \{\mathbf{q}^T \dot{\mathbf{q}}^T\}$,

$$\mathbf{A} = \begin{bmatrix} \mathbf{0} & \mathbf{I} \\ -\hat{\mathbf{M}}^{-1}\mathbf{K} & -\hat{\mathbf{M}}^{-1}\hat{\mathbf{C}} \end{bmatrix} \text{ and } \mathbf{B} = \begin{bmatrix} \mathbf{0} \\ \hat{\mathbf{M}}^{-1} \end{bmatrix}.$$

Then, according to the optimal control approach, the criterion for aeroelastic stabilization relies, for arbitrary weight matrices \mathbf{Q} and \mathbf{R} , on the identification of the relationship between \mathbf{f} and \mathbf{x} that minimizes the cost function

$$\mathcal{J} = \frac{1}{2} \int_0^{t_f} (\mathbf{x}^T \mathbf{Q} \mathbf{x} + \mathbf{f}^T \mathbf{R} \mathbf{f}) dt,$$

under constraint of satisfaction of equation (3). This procedure yields the following optimal control law

$$\mathbf{f} = -\mathbf{R}^{-1} \mathbf{B}^T \mathbf{S} \mathbf{x} = -\mathbf{G} \mathbf{x}, \quad (4)$$

where the $3N \times 6N$ feedback gain matrix, \mathbf{G} , is known once the solution of the algebraic Riccati equation, matrix \mathbf{S} , has been evaluated.

Now, it is possible to identify the ‘smart spring’ stiffness parameters. Indeed, the effect of the

‘smart spring’ stiffness is equivalent to the stabilizing optimal feedback gain matrix if

$$\Delta\mathbf{K}(\lambda_s^y, \lambda_s^z, \kappa_s) \mathbf{q} = \mathbf{G} \mathbf{x} = \mathbf{G}_1 \mathbf{q} + \mathbf{G}_2 \dot{\mathbf{q}}, \quad (5)$$

where \mathbf{G}_1 and \mathbf{G}_2 are two $3N \times 3N$ matrices, respectively composed of the first $3N$ columns and the last $3N$ columns of \mathbf{G} . Therefore, in order to determine matrix $\Delta\mathbf{K}$ it is necessary to express $\dot{\mathbf{q}}$ in terms of \mathbf{q} (*i.e.*, it is necessary to define a sort of observer for the $\dot{\mathbf{q}}$ variables). Here, assuming the low-frequency approximation for an observer dynamics obtained by combining equation (4) and equation (2) with \mathbf{f} as forcing term, and neglecting mass-matrix contributions, we have the following reconstruction for $\dot{\mathbf{q}}$

$$\dot{\mathbf{q}} = -[(\mathbf{G}_2 + \hat{\mathbf{C}})^{-1}(\mathbf{G}_1 + \mathbf{K})] \mathbf{q} = -\mathbf{H} \mathbf{q},$$

that in turns yields (see equation (5))

$$\Delta\mathbf{K}(\lambda_s^y, \lambda_s^z, \kappa_s) = \mathbf{G}_1 - \mathbf{G}_2 \mathbf{H}. \quad (6)$$

Finally, once the optimal ‘smart spring’ feedback matrix, $\Delta\mathbf{K}$, is determined, through a least square approach, it is possible to evaluate the ‘smart spring’ stiffness parameters, namely λ_s^y , λ_s^z and κ_s , as those that better satisfy the $3N \times 3N$ algebraic equations arising from the matricial equivalence in equation (6).

4. Numerical results

For the numerical validation of the algorithm for identification of stabilizing ‘smart spring’ properties, we have considered a four-bladed rotor, having radius $R = 2\text{m}$ and blade chord $c = 0.121\text{m}$ (that correspond to a solidity ratio $\sigma = 0.077$), and rotating with angular velocity $\Omega = 110\text{rad/sec}$. Furthermore, the Lock number considered is $\gamma = 5.0$, and the basic-blade elastic properties are $\lambda^y = EI^y/m\Omega^2 R^4 = 0.0017$, $\lambda^z = EI^z/m\Omega^2 R^4 = 0.0222$, and $\kappa = GI/m\Omega^2 R^4 = 0.001$ (see Appendix A for definition of blade structural parameters), whereas the piezoelectric material is located between $x_1/R = 0.05$ and $x_2/R = 0.2$.

First, we have analyzed the case with no flap-lag structural coupling (*i.e.*, following the notation in Ref. [9], $\mathcal{R} = 0$), for which the basic blade, in the precone/collective-pitch plane of Figure 4, shows a lead-lag flutter instability in the regions bounded by the crosses, and a divergence instability in the cross-filled area corresponding to high collective-pitch/small precone angles. Applying the ‘smart spring’ with the elastic properties predicted by the optimal procedure presented above, both flutter and divergence instabilities are considerably reduced, as depicted in Figure 5, where

the ‘smart’ blade instability regions are represented by circles. The effect of the ‘smart spring’ on the blade dynamics has also been analyzed in terms of root-loci modifications. Specifically, Figure 6 depicts, for precone angle $\beta_{pc} = 0.2\text{rad}$, the locus of the unstable (lead-lag) root for the collective-pitch angle $\theta = -0.1 \div 0.5\text{rad}$, and it is apparent as the ‘smart spring’ effect is to restrict considerably both the pitch-angle range for which flutter occurs and the maximum flutter excitation reachable.

The same blade, but for $\mathcal{R} = 1$, has also been examined. In this case, the basic-blade instability pattern on the precone/collective-pitch plane is more complicated, as illustrated in Figure 7 where, in addition to lead-lag flutter, torsion-flutter regions are also present (divergence instability would occur for configurations already experiencing torsional flutter). For this blade, the introduction of the optimal ‘smart spring’ considerably reduces both lead-lag and torsion flutter, as shown in Figure 8, where for the portion of the precone/collective-pitch plane considered, two of the four flutter instability regions have disappeared (circles bound ‘smart blade’ flutter regions). Finally, in Figure 9 we depict, for $\beta_{pc} = 0.2\text{rad}$ and for $\theta = -0.1 \div 0.5\text{rad}$, the lead-lag root locus with and without ‘smart spring’ effects. Also in this case, the smart spring restricts considerably both the pitch-angle range for which flutter occurs and the maximum negative damping.

Concluding remarks

The effects of the inclusion of a root ‘smart spring’ in a hingeless helicopter rotor blade have been investigated. First, an aeroelastic ‘smart’ blade model has been developed and then, it has been proposed an algorithm for the tailoring, at a given rotor configuration, of the optimal ‘smart spring’ addressed to aeroelastic stability augmentation. The resulting ‘smart spring’ optimal parameters can be considered as the tuning parameters of a ‘smart spring’ tunable dependently of the rotor configuration to be stabilized.

Numerical results concerning two hovering rotor configurations have demonstrated the capability of this algorithm to identify a ‘smart spring’ that considerably augment rotor blade stability.

In the case examined here, only three ‘smart spring’ (stiffness) parameters have been included in the optimization procedure, but the algorithm is applicable to more general cases, in which additional ‘smart spring’ parameters like, for instance, mass cross-section distribution and spanwise extension could be included in the identification process.

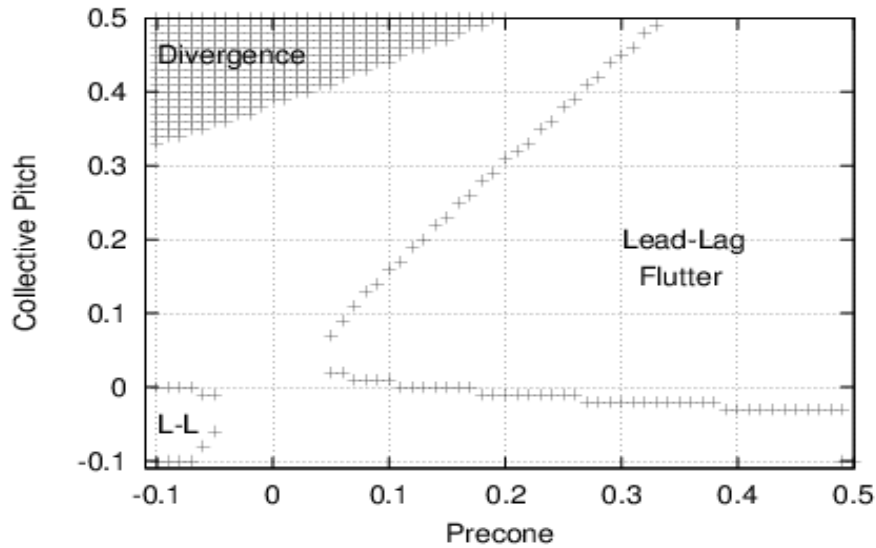


Figure 4: Instability regions for basic blade. $\mathcal{R} = 0$.

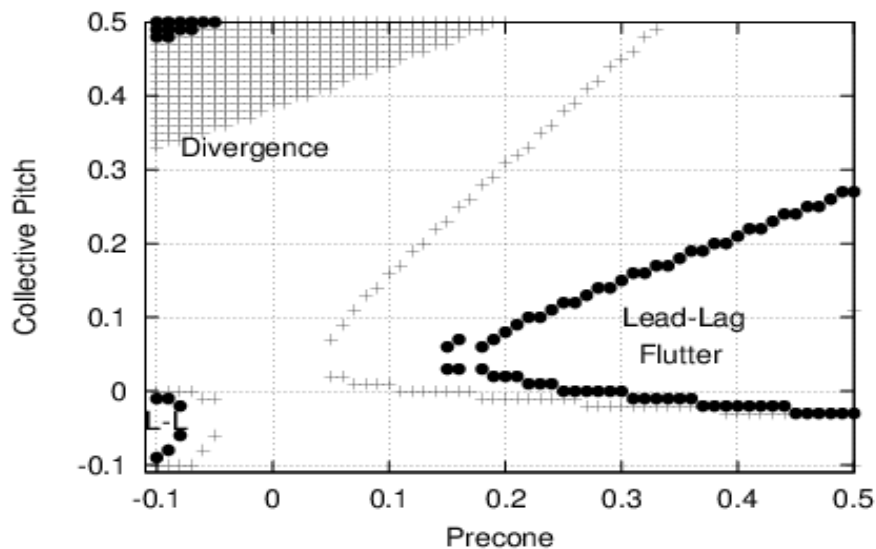


Figure 5: Instability regions for basic and 'smart' blades. $\mathcal{R} = 0$. (+:basic-blade instability boundaries; •:smart-blade instability boundaries)

References

- [1] Fulton, M. V. and Ormiston, R. A., Hover Testing of a Small-Scale Rotor with On-blade Elevons, *J. of American Helicopter Society*, 46, 2001, pp.96-106.
- [2] Wilbur, L. M., et al, Vibratory Loads Reduction Testing of the NASA/Army/MIT Active Twist Rotor, *J. of American Helicopter Society*, 47, 2002, pp.123-133.
- [3] Chopra, I., Status of Application of Smart Structures Technology to Rotorcraft Systems, *J. of American Helicopter Society*, 45, 2000, pp.228-252.
- [4] Nitzsche, F., Grewal, A. and Zimcik, D., Structural Component having Means for Actively Varying its Stiffness to Control Vibrations, U.S. Patent No. 5,973,440. Also European patent EP-996570-B1, 1999. 2001.
- [5] Nitzsche, F., Designing an Active Impedance Control Device to Actively Control Helicopter Blade Vibration, *CEAS/AIAA International Forum Aeroelasticity and Structural Dynamics*, Vol. 3, Madrid, Spain, 2001.
- [6] Kretz, M., Research in Multicyclic and Active Control of Rotary Wings, *Vertica*, 1, 1976, pp. 95-105.

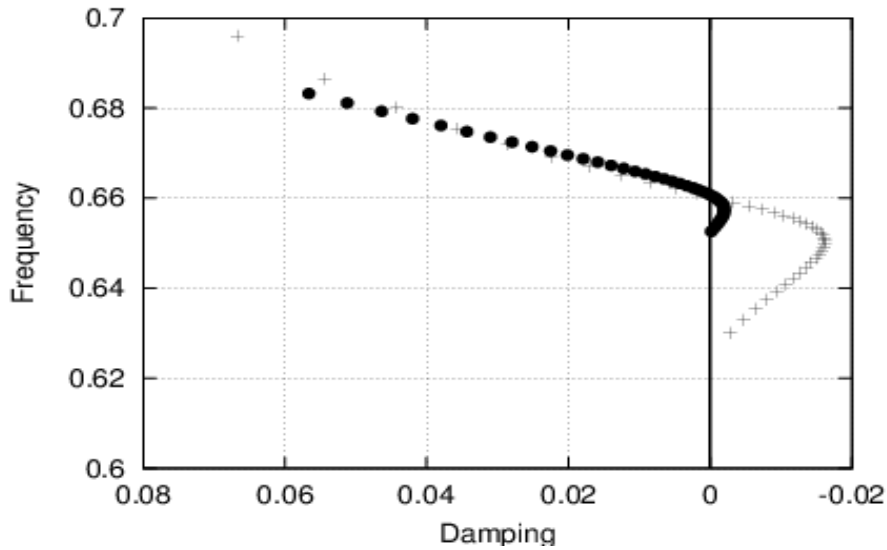


Figure 6: Critical lead-lag root locus for basic and ‘smart’ blades, at $\beta_{pc} = 0.2\text{rad}$ and $\theta = -0.1 \div 0.5\text{rad}$. $\mathcal{R} = 0$. (+:basic-blade root locus; •:smart-blade root locus)

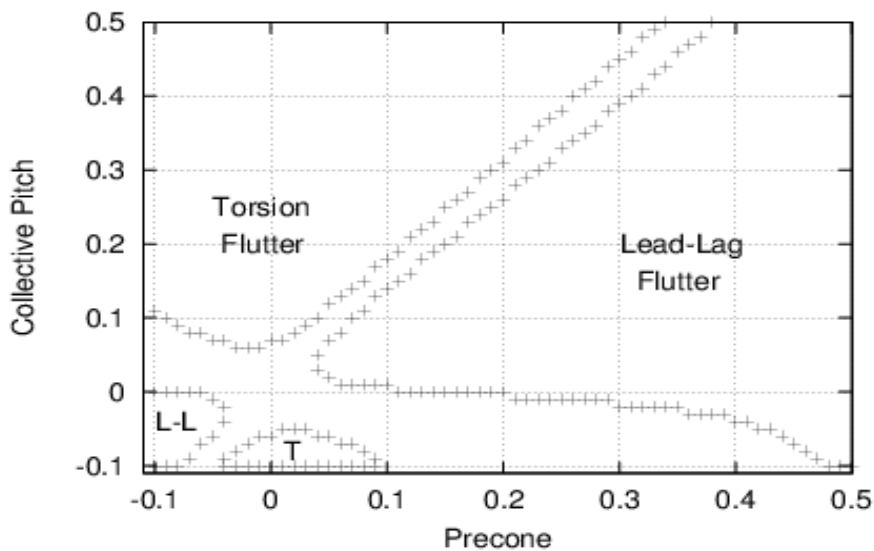


Figure 7: Instability regions for basic blade. $\mathcal{R} = 1$.

- [7] Zimcik, D. G., Wickramasinghe, V. K., Young, C. and Nitzsche, F., ‘Smart Spring’ Concept For Active Vibration Control In Helicopters, AHS International 58th Annual Forum and Technology Display, Montreal, Canada, 2002.
- [8] Solaiman, S., Afagh, F.F, and Nitzsche, F., An Investigation of the Aeroelastic Stability of a Helicopter Blade with a ‘Smart’ Spring at the Root, 25th European Rotorcraft Forum, Rome, Italy, 1999.
- [9] Hodges, D.H., and Ormiston, R.A., Stability of Elastic Bending and Torsion of Uniform Cantilever Rotor Blades in Hover with Variable Structural Coupling, NASA TN D-8192, 1976.
- [10] Greenberg, J.M., Airfoil in Sinusoidal Motion in a Pulsating Stream, NACA TN-1326, 1947.
- [11] Hodges, D.H., and Dowell, E.H., Nonlinear Equation of Motion for the Elastic Bending and Torsion of Twisted Nonuniform Rotor Blades, NASA TN D-7818, 1974.
- [12] Poloni, L., Studio di un Sistema di Smorzatori Passivi per la Stabilizzazione Aeroelastica di Rotori di Elicottero, Tesi di Laurea, University Roma Tre, 2001. (in italian)

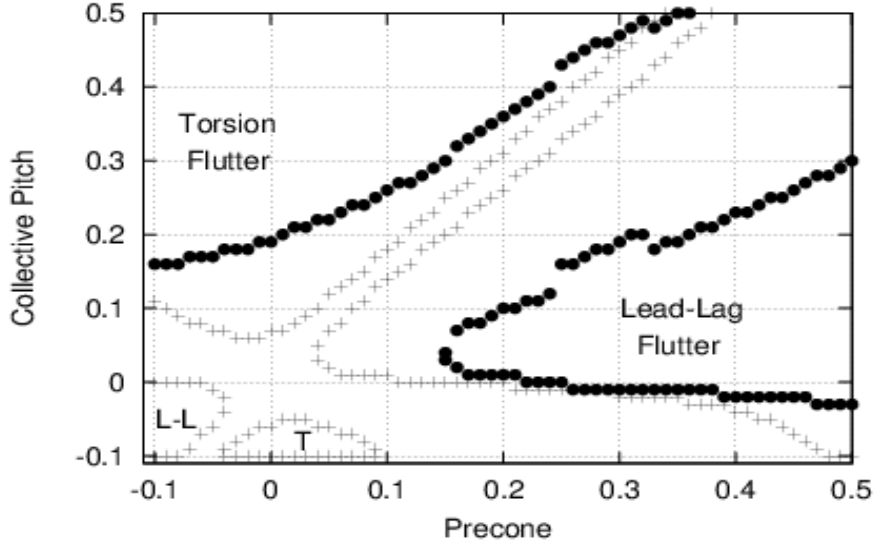


Figure 8: Instability regions for basic and ‘smart’ blades. $\mathcal{R} = 1$. (+:basic-blade instability boundaries; •:smart-blade instability boundaries)

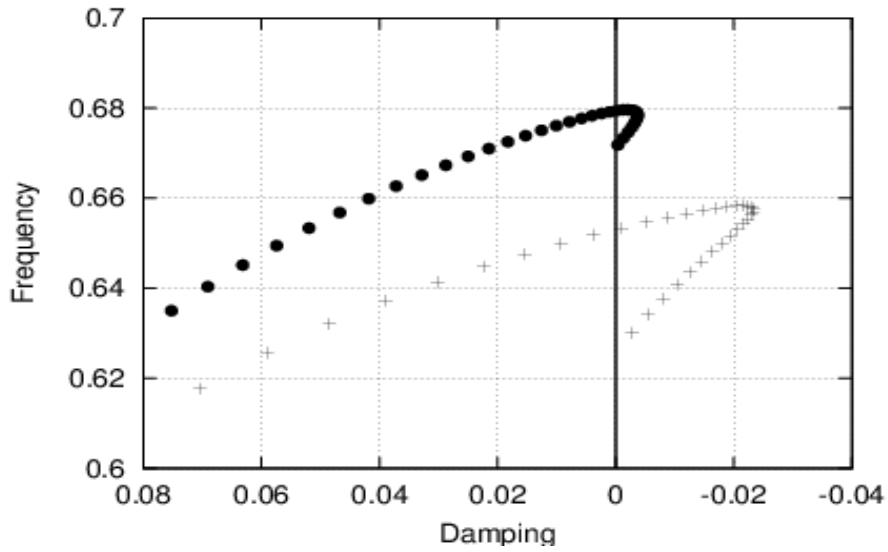


Figure 9: Critical lead-lag root locus for basic and ‘smart’ blades, at $\beta_{pc} = 0.2\text{rad}$ and $\theta = -0.1 \div 0.5\text{rad}$. $\mathcal{R} = 1$. (+:basic-blade root locus; •:smart-blade root locus)

Appendix A

For the sake of completeness, in this appendix we show the expressions of the ‘smart’ blade dynamics equations, as they have been derived in Ref. [12]. These are the equations that, after application of the Galérkin method, yield the state-

space format of ‘smart’ blade dynamics that has been used in the optimal-control procedure, for the ‘smart spring’ tailoring (as described in Section 3).

Using the notation introduced in Refs. [9] and [11], lead-lag, flap and torsion deformation equations have the following expressions:

(lead-lag equation)

$$\begin{aligned}
& -\frac{m_0\Omega^2}{2} [(R^2 - x^2) v']' - m_s\Omega^2 \left[v' \int_x^R \Delta H x dx \right]' - 2m_0\Omega \left[v' \int_x^R \dot{v} dx \right]' - 2m_s\Omega \left[v' \int_x^R \Delta H \dot{v} dx \right]' \\
& + \left\{ (E_0I_0^z - E_0I_0^y) \left[\phi \cos(2\mathcal{R}\theta) + \frac{\sin(2\mathcal{R}\theta)}{2} \right] w'' + \Delta H (E_sI_s^z - E_sI_s^y) \left[\phi \cos(2\mathcal{R}\theta) + \frac{\sin(2\mathcal{R}\theta)}{2} \right] w'' \right. \\
& + [E_0I_0^z (\cos^2(\mathcal{R}\theta) - \phi \sin(2\mathcal{R}\theta)) + E_0I_0^y (\sin^2(\mathcal{R}\theta) + \phi \sin(2\mathcal{R}\theta))] v'' + \Delta H [E_sI_s^z (\cos^2(\mathcal{R}\theta) - \phi \sin(2\mathcal{R}\theta)) \\
& + E_sI_s^y (\sin^2(\mathcal{R}\theta) + \phi \sin(2\mathcal{R}\theta))] v'' \left. \right\}'' + (m_0 + \Delta H m_s) \ddot{v} - 2(m_0 + \Delta H m_s) \Omega \beta_{pc} \dot{v} - (m_0 + \Delta H m_s) \Omega^2 v \\
& - 2(m_0 + \Delta H m_s) \Omega \int_0^x (v' \dot{v} + w' \dot{w}') dx = \mathcal{L}_v
\end{aligned}$$

(flap equation)

$$\begin{aligned}
& -\frac{m_0\Omega^2}{2} [(R^2 - x^2) w']' - m_s\Omega^2 \left[w' \int_x^R \Delta H x dx \right]' - 2m_0\Omega \left[w' \int_x^R \dot{w} dx \right]' - 2m_s\Omega \left[w' \int_x^R \Delta H \dot{w} dx \right]' \\
& + \left\{ (E_0I_0^z - E_0I_0^y) \left[\phi \cos(2\mathcal{R}\theta) + \frac{\sin(2\mathcal{R}\theta)}{2} \right] v'' + \Delta H (E_sI_s^z - E_sI_s^y) \left[\phi \cos(2\mathcal{R}\theta) + \frac{\sin(2\mathcal{R}\theta)}{2} \right] v'' \right. \\
& + [E_0I_0^z (\sin^2(\mathcal{R}\theta) + \phi \sin(2\mathcal{R}\theta)) + E_0I_0^y (\cos^2(\mathcal{R}\theta) - \phi \sin(2\mathcal{R}\theta))] w'' \\
& + \Delta H [E_sI_s^z (\sin^2(\mathcal{R}\theta) + \phi \sin(2\mathcal{R}\theta)) + E_sI_s^y (\cos^2(\mathcal{R}\theta) - \phi \sin(2\mathcal{R}\theta))] w'' \left. \right\}'' \\
& + (m_0 + \Delta H m_s) \ddot{w} + 2(m_0 + \Delta H m_s) \Omega \beta_{pc} \dot{w} + (m_0 + \Delta H m_s) \Omega^2 \beta_{pc} w = \mathcal{L}_w
\end{aligned}$$

(torsion equation)

$$\begin{aligned}
& -(G_0I_0\phi' + \Delta H G_s I_s \phi')' + (m_0 + \Delta H m_s) \Omega^2 [k_{m2_0}^2 + \Delta H k_{m2_s}^2 - k_{m1_0}^2 - \Delta H k_{m1_s}^2] \phi \cos(2\theta) \\
& + [(E_0I_0^z - E_0I_0^y) + \Delta H (E_sI_s^z - E_sI_s^y)] \left[(w''^2 - v''^2) \frac{\sin(2\mathcal{R}\theta)}{2} + v'' w'' \cos(2\mathcal{R}\theta) \right] \\
& - \left[(k_{A_0}^2 + \Delta H k_{A_s}^2) \phi' \int_x^R (m_0 + \Delta H m_s) \Omega^2 x dx \right]' + (J_0 + \Delta H J_s) \ddot{\phi} \\
& + (m_0 + \Delta H m_s) \Omega^2 [k_{m2_0}^2 + \Delta H k_{m2_s}^2 - k_{m1_0}^2 - \Delta H k_{m1_s}^2] \frac{\sin 2\theta}{2} = \mathcal{M}_\phi
\end{aligned}$$

where $'$ denotes differentiation with respect to the abscissa, x , along the blade span, subscript 0 denotes basic-blade parameters, whereas subscript s denotes 'smart spring' parameters at $x_1 < x < x_2$. Furthermore, R denotes the rotor radius, Ω denotes the rotor angular velocity, m denotes the blade mass per unit length, J denotes the cross-section torsional mass moment of inertia, E denotes the Young modulus, G denotes the shear modulus, I^z and I^y are the cross-section area moment of inertia, I is the torsional rigidity

constant, k_A is the cross-section polar radius of gyration, whereas k_{m1} and k_{m2} are such that the cross-section mass radius of gyration, k_m , is given by $k_m^2 = k_{m1}^2 + k_{m2}^2$. In addition, \mathcal{R} is the flap-lag structural coupling parameter, θ is the collective pitch, β_{pc} is the blade precone angle, ΔH is the hat function defined in Section 3, whereas \mathcal{L}_v and \mathcal{L}_w are, respectively, the in-plane and out-of-plane aerodynamic forces per unit length acting on the blade, whereas \mathcal{M}_ϕ is the aerodynamic pitching moment per unit length.